



● *Original Contribution*

## STUDYING THE ORIGIN OF REVERBERATION CLUTTER IN ECHOCARDIOGRAPHY: *IN VITRO* EXPERIMENTS AND *IN VIVO* DEMONSTRATIONS

ALI FATEMI,\* ERIK ANDREAS RYE BERG,\*<sup>†</sup> and ALFONSO RODRIGUEZ-MOLARES\*

\* Department of Circulation and Medical Imaging, Norwegian University of Science and Technology, Trondheim, Norway; and

<sup>†</sup> Heart Clinic, St. Olavs Hospital, Trondheim, Norway

(Received 13 July 2018; revised 7 January 2019; in final form 12 January 2019)

**Abstract**—Clutter in echocardiography hinders the visualization of the heart and reduces the diagnostic value of the images. The detailed mechanisms that generate clutter are, however, not well understood. We present five different hypotheses for generation of clutter based on reverberation artifact with a focus on apical four-chamber view echocardiograms. We demonstrate the plausibility of our hypotheses by *in vitro* experiments and by comparing the results with *in vivo* recordings from four volunteers. The results show that clutter in echocardiography can be originated both at structures that lie in the ultrasound beam path and at those that are outside the imaging plane. We show that reverberations from echogenic structures outside the imaging plane can make clutter over the image if the ultrasound beam gets deflected out of its intended path by specular reflection at the ribs. Different clutter types in the *in vivo* examples show that the appearance of clutter varies, depending on the tissue from which it originates. The results of this work can be applied to improve clutter reduction techniques or to design ultrasound transducers that give higher quality cardiac images. The results can also help cardiologists have a better understanding of clutter in echocardiograms and acquire better images based on the type and the source of the clutter. (E-mail: [ali.fatemi@ntnu.no](mailto:ali.fatemi@ntnu.no)) © 2019 The Author(s). Published by Elsevier Inc. on behalf of World Federation for Ultrasound in Medicine & Biology. This is an open access article under the CC BY-NC-ND license. (<http://creativecommons.org/licenses/by-nc-nd/4.0/>).

**Key Words:** Cardiac ultrasound, Echocardiography, Clutter, Reverberation, Specular reflection.

### INTRODUCTION

Cardiovascular disease is the leading cause of death globally (World Health Organization 2018). An important factor in reducing mortality rate is early diagnosis. Echocardiography provides a non-invasive, comprehensive evaluation of the heart structure and function (Gottdiener et al. 2004). However, echocardiography does not provide optimal images in all patients. Following low quality images, it can be difficult or impossible to identify crucial findings, which may lead to failure of correctly diagnosing large subsets of patients. In a study on accuracy of transthoracic echocardiography (TTE) (Chirillo et al. 2004), only 62% of 139 patients suspected of having infective endocarditis were correctly diagnosed by fundamental B-mode imaging.

Acoustic clutter is a major problem in several applications. Post-formation image processing techniques, such as

image segmentation (Noble and Boukerroui 2006) and motion analysis (Ledesma-Carbayo et al. 2006) have been attempted on cardiac ultrasound images. However, high levels of clutter limit effectiveness of such techniques in a considerable proportion of cardiac data sets (Perperidis 2016). Additionally, clutter inhibits visualization of abnormalities, such as tumors and vegetations (Bell et al. 2012). It is widely accepted that aberration and reverberation are the two main causes of acoustic clutter. Over the years, a number of studies have investigated the origins of these two artifacts, and several approaches have been introduced to remove clutter from cardiac ultrasound images.

Ultrasonic wavefront distortion caused by the abdominal wall has been studied through *ex vivo* experiments (Hinkelman et al. 1998) and simulations (Mast et al. 1998) using specimens of the upper abdominal wall. In these studies, the effect of the subcutaneous fat and muscle on the ultrasonic pulse was investigated. In similar studies, Hinkelman et al. (1997) and Mast et al. (1999) measured the distortion of the ultrasonic pulse by the human chest wall. Arrival time and energy level fluctuations caused by

Address correspondence to: Ali Fatemi, AHL-senteret, 343.03, K03, Øya, Prinsesse Kristinas gt. 3, Trondheim, Norway. E-mail: [ali.fatemi@ntnu.no](mailto:ali.fatemi@ntnu.no)

soft tissue and bone were calculated in these studies through measurements and simulations. Several methods (Fink 1992; Lin and Waag 2002; Liu and Waag 1994) have been proposed to correct for these distortions.

When it comes to reverberation, there are few studies describing the sources and mechanisms of clutter generation. Dahl and Sheth (2014) studied the relation between the reverberation clutter magnitude and the angle and density of connective tissue in simplified 2-D simulation models. They also showed that the reverberation clutter decays faster when compression is applied. In another study (Pinton et al. 2011), the propagation of ultrasound in the human abdomen was studied using finite difference simulations. The results of this study show that reverberation is mostly responsible for clutter in fundamental images, while aberration is the dominant source of clutter in harmonic images. In the mentioned studies, however, 2-D simulation was used, and therefore the effect of out-of-scan-plane sources on reverberation clutter was ignored. Furthermore, the effect of highly reflective tissue, such as bone and lung, has not been studied.

Different methods have been proposed to correct for reverberation clutter. The most successful method has been harmonic imaging (HI), which has become the *de facto* standard in commercial echographic systems (Matte et al. 2011). HI is an imaging modality based on transmitting ultrasound at a given frequency and receiving echoes at twice the transmitted frequency. Initially applied to contrast echocardiography (Porter and Xie 1995), HI was later found beneficial to improve image quality even without the use of contrast agents (Spencer et al. 1998). HI provides lower side-lobe level compared with fundamental imaging, making it less sensitive to off-axis scatterers. Additionally, because the harmonic energy builds up progressively, HI reduces the effects of multiple reflections and near-field artifacts (Matte et al. 2011). By reducing the number of poor and suboptimal quality images, HI improves the diagnostic value of TTE. This has been shown by Chirillo et al. (2004), where HI led to an increase in the rate of correct diagnoses from 62% to 90%. However, it still leaves a subset of patients with low-quality images that inhibit correct diagnosis. Results of another study on patients in the intensive care unit after cardiac surgery (Flynn et al. 2010) show inadequate visualization of the left ventricle in 17% of patients using harmonic TTE.

Ultrasound contrast agents (Goldberg et al. 1994) enhance the contrast between blood and the heart tissue during echocardiography and therefore increase the diagnostic value of TTE examinations. According to a study on a group of 632 patients with technically difficult echocardiographic studies without contrast agents, using intravenous contrast gave adequate echocardiograms in 90% of the patients (Kurt et al. 2009). Early

concerns on the safety profile of these agents were later played down following the very low rates of reported serious events (Main 2009; Wei et al. 2008). However, the approach presents additional costs and requires intravenous access.

Post processing techniques and adaptive beamforming are other approaches to reduce clutter and increase the image contrast. In a recent study, Perperidis (2016) reviewed and classified post-processing techniques. Seo and Yen (2008) used two different receive apodizations on the same data set and reduced the side-lobe levels by cross-correlating data without compromising lateral resolution. By reducing the clutter generated by side lobes, this method increases the image contrast. Coherence-based beamforming methods, such as short-lag spatial coherence (Lediju et al. 2011), that take advantage of the similarity of the echo's wavefront to separate speckle and clutter can suppress aberration and reverberation artifacts.

To our knowledge, there has not been a systematic study on detailed mechanisms that generate reverberation clutter in transthoracic cardiac images and the appearance of the clutter based on how it is generated. Performing such a study is highly beneficial to evaluate the potential of clutter-reduction techniques for improving the quality of transthoracic cardiac images. In this paper, we try to address this by presenting five scenarios that can result in generation of reverberation clutter in apical four-chamber view echocardiograms. We simulate each of these scenarios by water tank experiments with synthetic materials and biological tissues. Finally, we compare the results of the experiments with *in vivo* recordings from four volunteers in order to understand the relation between the appearance of clutter and the mechanism that generates it.

## THEORY

Videos 1 and 2 display two apical four-chamber view echocardiographic loops in harmonic mode. The echocardiograms are recorded, using an M5Sc-D transducer connected to a Vivid E95 (GE Vingmed Ultrasound AS, Horten, Norway) scanner, from two volunteers. The loops are acquired in harmonic mode with 1.7 MHz transmit and 3.3 MHz receive frequency. The echocardiogram of volunteer A (Video 1) shows an example of a good quality echocardiogram, where there is a high contrast between blood and heart tissue all over the sector. In contrast, the echocardiogram of volunteer B (Video 2) shows an example of a cluttered echocardiogram. In this case, a band of clutter around 5-cm depth reduces the contrast of this region and hinders the visualization of the heart walls.

In cardiac ultrasound images, clutter appears as a consequence of interaction between the transmitted signal and structures within the examined body (Perperidis 2016). These

interactions mostly result in multiple reflections (known as reverberations) that are received by the transducer and rendered as clutter over the image because of the intrinsic pitfalls of beamforming (conventional beamforming assumes there is only scattering and no multiple reflections). We study five scenarios (shown by the five drawings in Fig. 1) that result in different types of clutter noise. These scenarios are based on reverberations from echogenic structures in the left thoracic region. What we present here is therefore not an exhaustive list of clutter generation mechanisms; for example, those that are solely based on side lobes or grating-lobes are not included here. Potential echogenic structures are skin, subcutaneous fat, bone and cartilage, intercostal muscle, lung and out-of-scan-plane heart tissue.

In order to acquire a transthoracic echocardiogram, ultrasound energy has to pass through layers of skin, subcutaneous fat and intercostal muscle before reaching the heart. While taking this path, part of the energy can be reflected several times at the interfaces between these layers and received by the transducer, resulting in reverberation noise. This is considered the most common source of near-field clutter that is mostly removed by HI. Figure 1a illustrates this scenario (case I), where a phased array transducer is shown in the azimuth direction while taking an apical four-chamber view image of the heart. This drawing shows some of the possible reflection paths that result in reverberation. When there is a thicker layer of fat and muscle under the skin, more harmonic energy is built up, making it difficult to remove the clutter using HI. This mechanism can explain the higher clutter level in patients with higher body mass index even when HI is used.

In patients where the heart apex is partially covered by the left lung, reverberations from lung tissue are the most plausible source of clutter noise. In this case, part of the ultrasound energy encounters the left lung before reaching the heart. Reverberations generated between the air-filled cavities (alveolar sacs) of the lung travel back to the transducer and form clutter over the heart image. Figure 1 (b, c) shows two scenarios where the heart is partially covered by the lung in azimuth and elevation directions, respectively (case II and case III, respectively). In case II, one side of the echocardiogram will be cluttered because of the reverberations originating at the lung. This type of clutter is easy to identify as it moves in and out of the image sector in the azimuth direction while the patient breathes. In case III, the whole image is cluttered since the transmit beams partially hit the lung, regardless of the azimuth direction they are sent. This clutter flickers with the respiration and is not completely removed by HI.

In order to get a clear image of the heart, the ultrasound beam should be transmitted and received between the ribs with as little interaction with the ribs as possible. Difficult-to-image patients may have a shorter

intercostal distance or an adverse relative location of the heart and ribs. In those patients, the ultrasound beam does not intersect the heart in the desired view without interfering with the ribs. In the case of the apical four-chamber view, the beam may be partially blocked by the ribs in the elevation direction and get reflected out of its intended path because of specular reflection at the surface of the ribs. Depending on the beam-to-rib angle, this reflection of energy can be either inside or outside the ribcage.

In Figure 1 (d, e), the ultrasound beam is partly blocked in the elevation direction (shown by red color). After hitting the rib in Figure 1d (case IV), the ultrasound energy is reflected outside the ribcage. This energy may reach the fat and skin layers, where it is reverberated and reflected back to the transducer either directly or *via* a second specular reflection at the rib. This energy will then be rendered as a static clutter over the image of the heart. This mechanism may be a prevalent cause of clutter in patients with a small acoustic window between the ribs and a high body mass index.

In Figure 1e (case V), the blocked part of the beam is deflected from its intended path but still reflected inside the ribcage because of a smaller incident angle with the rib. This deflected energy may reach either the out-of-scan-plane heart tissue or the left lung, where it is reverberated between the alveolar sacs. These reverberations will then travel back to the ultrasound transducer *via* a second specular reflection at the rib and be rendered on top of the heart image as clutter noise. The reverberations from the lung flicker with respiration, while the reverberations from out-of-scan-plane heart tissue move with the heart cycle. The clutter in case IV and case V cannot be totally removed by HI because of long pulse-travel distance.

It should be noted that the scenarios presented in this section are potential mechanisms for explaining the formation of clutter in apical four-chamber view echocardiograms. A combination of these mechanisms can occur in one examination. Therefore, it is not always easy to identify the exact origin of clutter.

## MATERIALS AND METHODS

To validate the plausibility of the scenarios presented in the theory section, we carried out watertank experiments with synthetic materials and biological tissues. All experimental data were acquired with an M5Sc-D transducer connected to a Vivid E95 scanner. Fundamental ultrasound images were recorded at 2 MHz center frequency, and harmonic images were recorded using 1.7 MHz transmit and 3.3 MHz receive frequency.

A synthetic ventricle was used to simulate the heart. The ventricle was made of 10% polyvinyl alcohol (PVA),

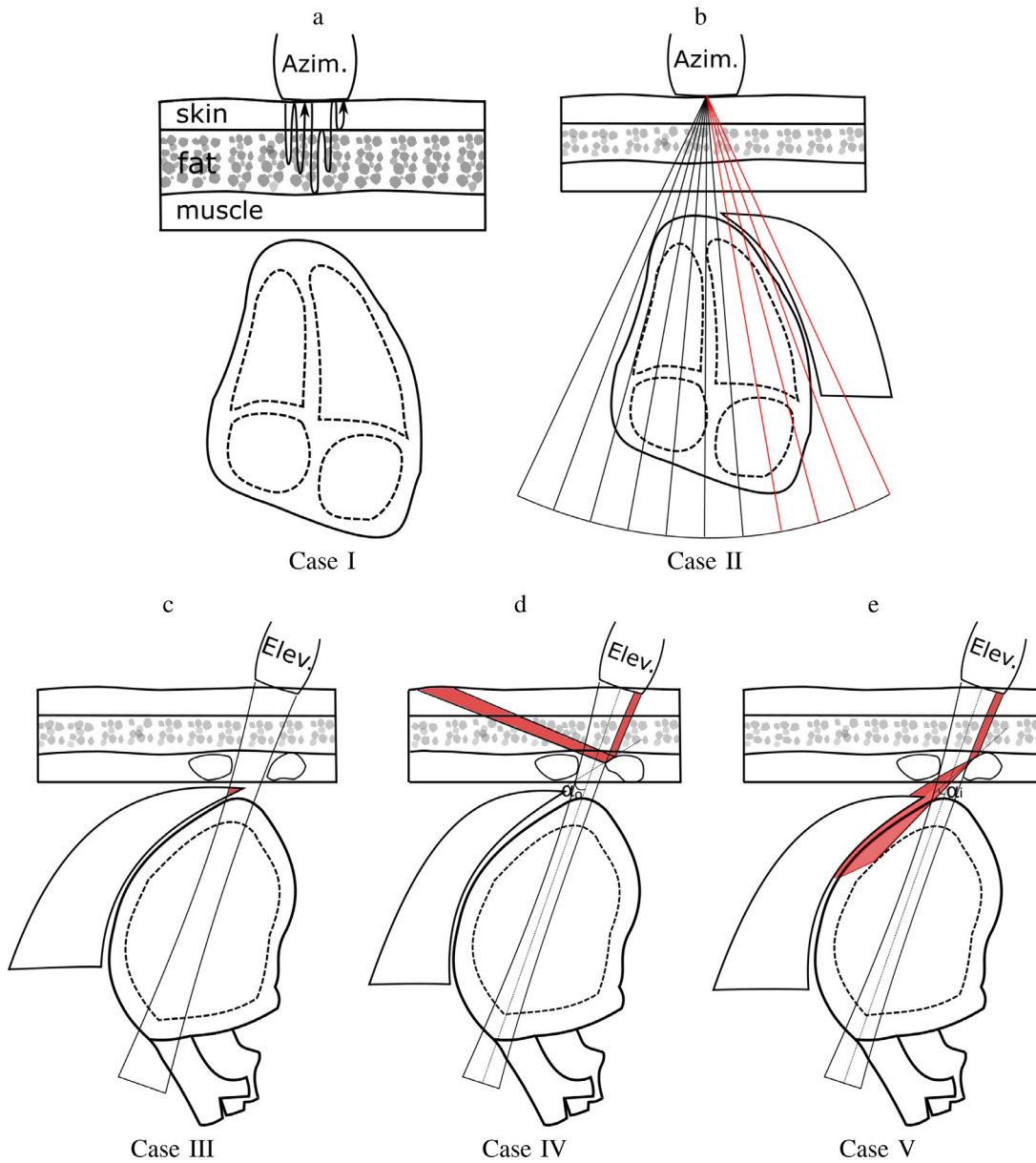


Fig. 1. Five possible scenarios for reverberation clutter generation while taking apical four-chamber view echocardiograms. Image (a) shows a phased array transducer in the azimuth direction placed on the patient’s skin. Under the skin layer, there is a layer of fat and a layer of muscle. The two arrows show two different paths that the ultrasound energy can take before being received by the transducer. Image (b) shows the same view as image (a) with a thinner layer of fat, and a part of the lung is drawn close to the heart. The diagonal lines from the transducer show the ultrasound beams sent in different directions to form the image. Where the heart apex is blocked by the lung, the ultrasound beam hits the lung before reaching the heart (illustrated by the red lines). Image (c) shows the transducer and the focused transmit beam in the elevation direction. The lung in this case is also partially blocking the ultrasound beam, this time in the elevation direction. The part of the lung that is hit by the beam before reaching the heart is shown in red. Image (d) shows the same view as image (c) with a shorter intercostal space. The focused beam in the elevation direction is partially blocked by the right rib. The blocked part of the beam is reflected at the rib and takes a new path toward the fat and skin layers (shown in red). The angle between the ultrasound beam and the rib surface is shown by  $\alpha_o$  in this case. Image (e) shows a similar scenario as image (d), except that the rib is hit at a different angle by the ultrasound beam ( $\alpha_i < \alpha_o$ ). Therefore, the blocked part of the beam takes a new path inside the chest toward the lung. Azim. = azimuth; Elev. = elevation direction.

10% glycerol for speed of sound matching, 1% graphite to increase scattering and 79% water. The glycerol and water were mixed in a beaker at room temperature, and the solution was heated while being stirred. The PVA was then added at 80°C. The mixture was then cooled down to 50°C, and the graphite was added. At 40°C, the solution was poured into a ventricle-shape mold. After three freeze/thaw cycles, 12/12 h each, the synthetic ventricle was unmolded. Figure 2 shows a picture of the ventricle aligned with its harmonic ultrasound image.

Pieces of pig ribs and layers of skin, muscle and fat were acquired from a slaughterhouse to simulate human ribs and chest wall. A piece of sponge was used to simulate the effect of lungs in ultrasound images. The air-filled cavities of the sponge represent the alveolar sacs within the lung. Hence, the sponge was squeezed carefully before each recording to get rid of the water trapped inside.

Figure 3 shows pictures taken of the water tank experiments. In the first experiment, shown by Figure 3a, layers of skin, fat and muscle with 10 and 20 mm thickness were placed in front of the transducer while imaging the ventricle. Pictures of the setups of this experiment in three different states are shown in Figure 4, where the dashed lines show the water level. In the second and third experiments, shown by Figure 3 (b, c), the sponge was held over the ventricle, partially blocking the ultrasound beam in the azimuth and elevation directions, respectively. Pictures of the setups of the second experiment are shown in Figure 5. In this experiment, the ventricle was once imaged by the transducer while they were both immersed under water, and in the second state, the sponge, with a thickness of 11 mm, was held between the transducer and the ventricle while partially blocking the transducer in the azimuth direction. In the third experiment, the sponge was placed in two different positions (shown in Fig. 6), partially blocking the transducer in the elevation direction. In state 3, the sponge was moved 3 mm to the right to block more of the ultrasound energy. In the last two experiments, shown by Figure 3 (d, e), two pig ribs were placed in front of the transducer, partially blocking the beam in the elevation direction to simulate case IV and case V. In both experiments, there was an

angle of about 50 degrees between the transducer and the ribs in order to simulate the angle between the transducer and the patient's chest while taking an apical four-chamber view echocardiogram. In the fourth experiment, the angle between the right rib surface and the ultrasound beam was 35 degrees (shown in Fig. 7 as  $\alpha_o$ ). In state 1 of this experiment, the ventricle was imaged by the transducer while a layer of skin, fat and muscle was placed above the ribs, and there was a 16-mm distance between the ribs. In state 2, the right rib was moved toward the left rib, reducing the distance to 14 mm. In state 3, the layer of skin, fat and muscle was removed. In state 4, this layer was placed back above the ribs, and the distance between the ribs was further reduced to 12 mm by moving the right rib. Finally, in state 5, the layer of skin, fat and muscle was again removed. In the fifth experiment, the right rib was rotated 20 degrees counterclockwise to get an angle of 15 degrees between the ultrasound beam and the right rib surface (shown in Fig. 9 as  $\alpha_i$ ). In state 1 of this experiment, the ventricle was imaged by the transducer while there was a 15 mm distance between the ribs and the sponge was held close to the ventricle under the left rib. In state 2, the right rib was moved toward the left rib, reducing the distance to 12 mm. In state 3, the sponge was removed, and finally, in state 4, the layer of skin, fat and muscle was placed above the ribs in a similar way to the fourth experiment. Three elliptic areas were marked in all ultrasound images of each state of these experiments to calculate the contrast ratio (CR) between the ventricular walls and the chamber. CRs are measured as the difference between the mean intensities of the right and left walls (marked by the yellow and cyan ellipses) and the mean intensity of the chamber (marked by the red ellipse). The only exception is experiment 2, in which the CR is calculated as the difference between the mean intensity of the right wall and the mean intensity of the chamber.

The elevational transmit beamprofile of the ultrasound transducer was measured by an Onda HNA-0400 hydrophone, mounted on a 3-D position system (Physik Instrumente GmbH & Co. KG, Karlsruhe, Germany). The beamprofile measurement was repeated four times while two pieces of pig ribs were placed in front of the

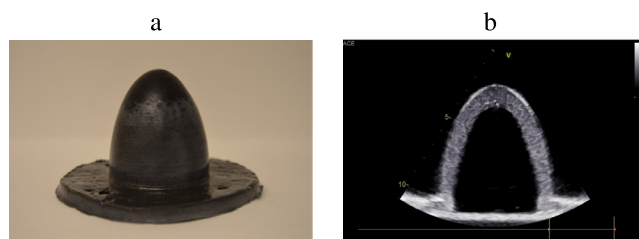


Fig. 2. Synthetic ventricle made of polyvinyl alcohol. Image (a) shows a picture taken of the ventricle by a DSLR camera; image (b) shows an ultrasound image of the same ventricle in a water tank acquired with an M5Sc-D transducer connected to a Vivid E95 scanner. DSLR = digital single-lens reflex.

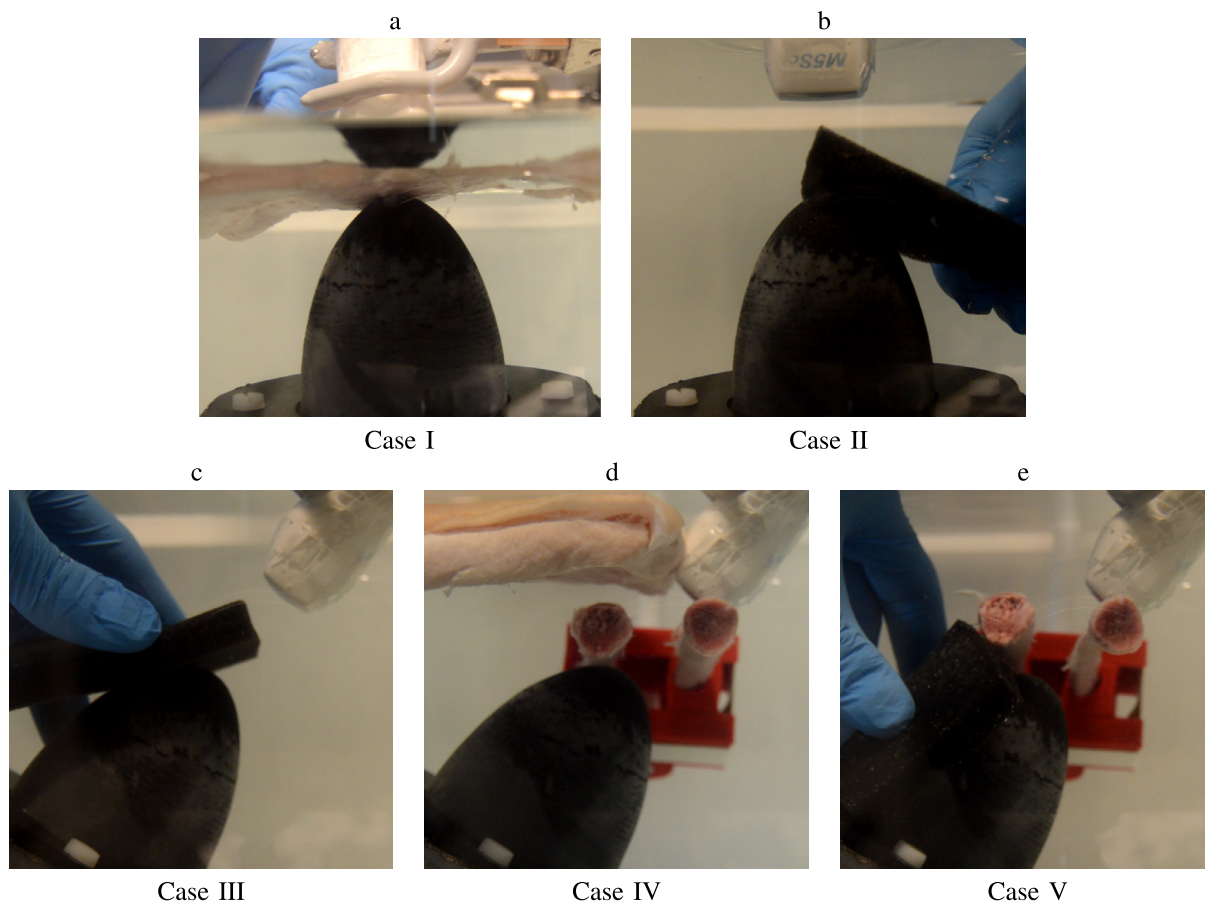


Fig. 3. Pictures taken of the water tank experiments carried out to reproduce clutter noise. (a) Experiment with a section of pig chest wall between the transducer and the synthetic ventricle; (b) the ventricle blocked by the sponge in the azimuth direction; (c) the ventricle blocked by the sponge in the elevation direction; (d) ribs blocking the beam in the elevation direction, deflecting it toward the tissue, which is placed above the ribs; (e) ribs blocking the beam in the elevation direction, deflecting it toward the sponge, which is held close to the ventricle.

transducer in four different states. All beamprofiles were recorded with a resolution of 2 mm. A picture of the setup is shown in Figure 8. In these measurements, the transducer was placed with an angle of about 50 degrees to the ribs in order to simulate the angle between the transducer and the patient's chest while acquiring an apical four-chamber view echocardiogram. The relative transducer-hydrophone position in all four measurements is identical. The position of the ribs and the distance between them were changed to study the effect of intercostal distance and beam-to-rib angle on the elevational beamprofile while taking an apical four-chamber view echocardiogram. The measured values in each state are normalized to the highest value of the first measurement, and the beamprofiles are shown in logarithmic scale with a dynamic range of 27 dB.

To compare the result of water tank experiments with *in vivo* examples, apical four-chamber view echocardiograms were recorded from four healthy volunteers. All

echocardiograms were recorded by the same clinician using a Vivid E95 scanner and an M5Sc-D transducer in harmonic mode using 1.7 MHz transmit and 3.3 MHz receive frequencies. Informed consents were received from all volunteers to use their images for publication. However, this type of recording does not need an approval by regional ethics committee since there is no comparison of diagnostics or interventions but only recordings by a commercial scanner in clinical mode as examples on different types of clutter. Videos 3 and 4 were acquired from volunteer A. In Video 3, the volunteer inhaled and held his breath, while in video 4, he was breathing normally. Video 5 was acquired from volunteer B while the clinician pushed on the volunteer's chest three times during the recording. The pushing was done gently and with one finger at about 5 cm distance from the transducer while the transducer was held still. Video 6 was acquired from volunteer C. Videos 7 and 8 were acquired from the same volunteer (volunteer D) with slightly different transducer positioning.

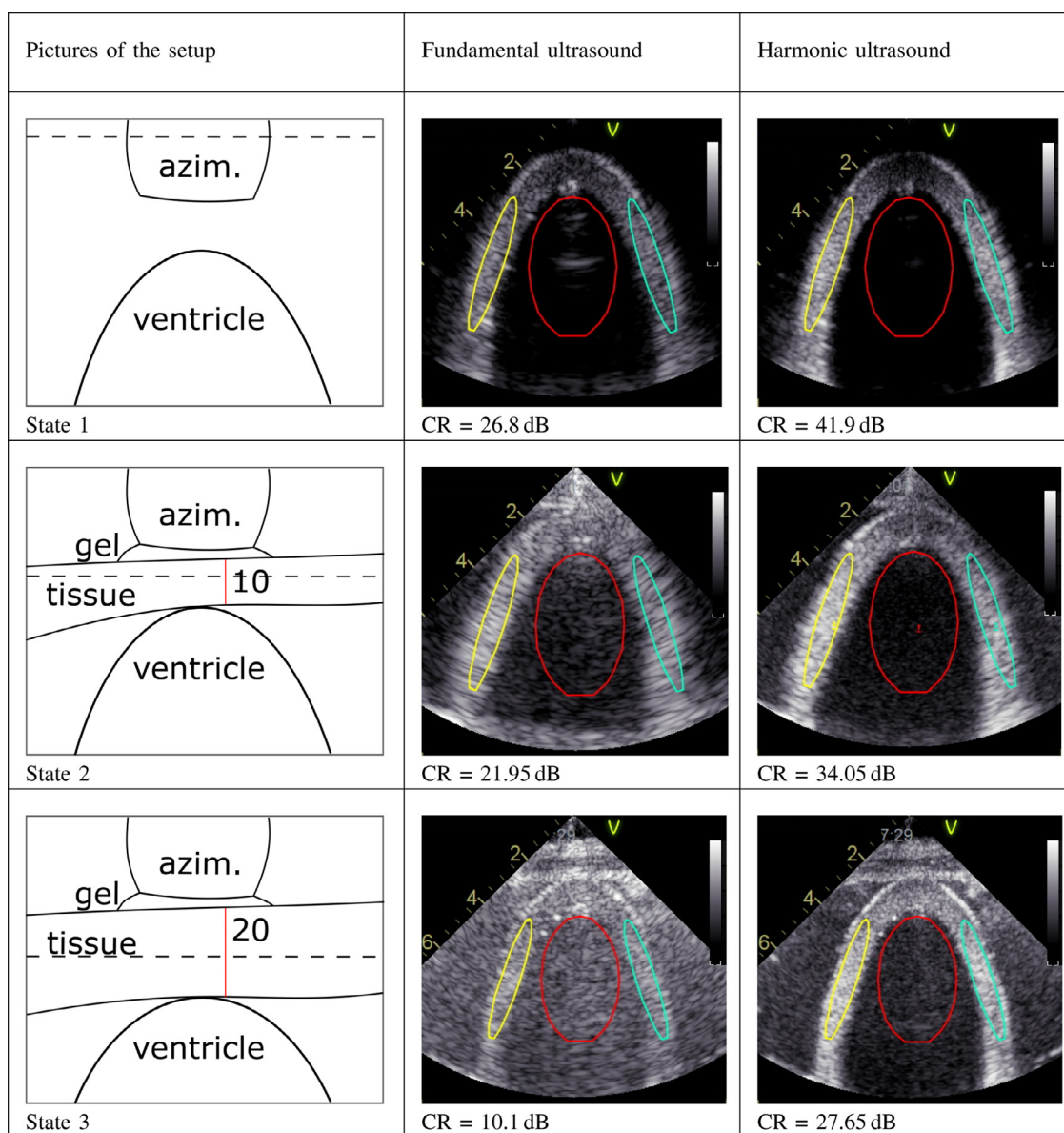


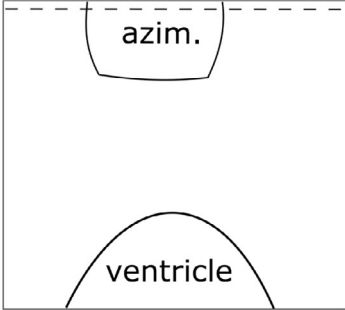
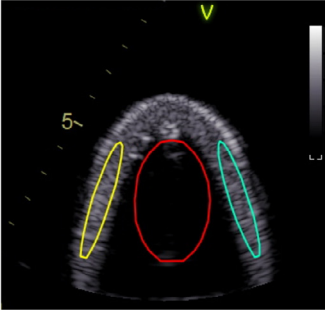
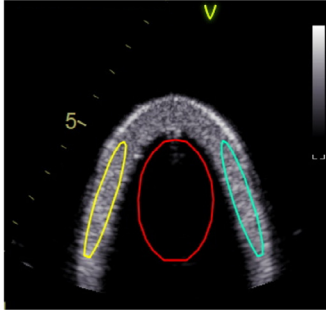
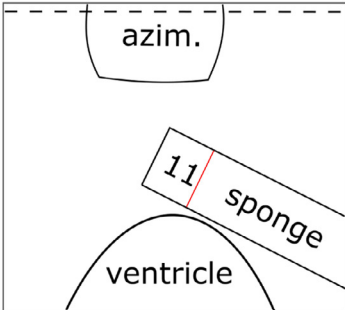
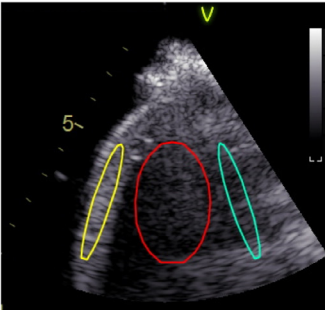
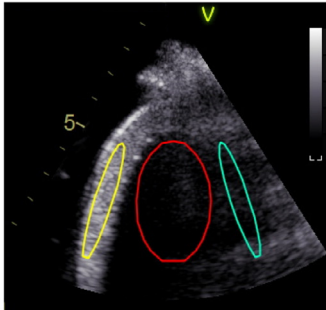
Fig. 4. Case I: Reproducing clutter noise in a water tank using complex layers of skin, fat and muscle, where a synthetic ventricle is imaged by an M5Sc-D transducer in three different states. A drawing of the setup in each state is shown in the first column. The thickness of the tissue layer is given in millimeters, and the water level is drawn by the dashed lines. Fundamental and harmonic ultrasound images taken in each state are shown in the second and third columns. Contrast ratios between the ventricle walls and the chamber are given under each ultrasound image. azim. = azimuth; CR = contrast ratio.

## RESULTS

Results from the water tank experiments for cases I to V are presented in [Figures 4 to 7](#) and [Figure 9](#). The first columns in these figures display drawings of the setups in different states with distances given in millimeters. The last two columns show the corresponding fundamental and harmonic ultrasound images.

Comparing ultrasound images of states 1 and 2 in [Figure 4](#) shows how adding 10 mm of skin, fat and muscle

in front of the transducer reduces the contrast of the images. However, the ventricle can still be clearly seen in both fundamental and harmonic images in state 2. Ultrasound images in state 3 show how changing the layer of fat and muscle to a 20-mm-thick layer further reduces the contrast. The ventricle is hardly visible in the fundamental ultrasound image in this case. HI removes some of the reverberations and gives a lower contrast image of the ventricle than state 2. The results in [Figure 5](#) show how reverberations coming from the lung can block the image of the

Pictures of the setup	Fundamental ultrasound	Harmonic ultrasound
 <p>State 1</p>	 <p>CR* = 26.4 dB</p>	 <p>CR* = 38.9 dB</p>
 <p>State 2</p>	 <p>CR* = 5.6 dB</p>	 <p>CR* = 5.5 dB</p>

\*The CR in this case is calculated as the contrast ratio between the right wall (cyan) and the chamber (red).

Fig. 5. Case II: Reproducing clutter noise in a water tank using a piece of sponge in azimuth to simulate the effect of the lung. A synthetic ventricle is imaged by an M5Sc-D transducer in two different states. A drawing of the setup in each state is shown in the first column. The thickness of the sponge is given in millimeters, and the water level is drawn by the dashed lines. Fundamental and harmonic ultrasound images taken in each state are shown in the second and third columns. Contrast ratios between the right ventricle wall (cyan) and the chamber (red) are given under each ultrasound image. *azim.* = azimuth; CR = contrast ratio.

heart. In Figure 6, comparing ultrasound images of states 2 and 3 shows how the clutter increases and the image contrast deteriorates as the sponge is moved 3 mm to the right and blocks more of the ultrasound beam in the elevation direction. HI in this case removes some of the clutter and increases the image contrast. In the fourth experiment (Fig. 7), the situation presented by Figure 1d was experimentally demonstrated in a water tank. The fundamental and harmonic images in state 1 show clear images of the ventricle since there is not enough energy being deflected toward the tissue. In state 2, more of the beam is blocked and deflected toward the tissue, which is placed above the ribs. In the fundamental ultrasound image, the ventricle is covered by clutter originating at the tissue after specular reflection at the ribs, decreasing CR to 4.4 dB. HI removes part of the clutter, making it possible to visualize the ventricle. Note the reflections from the ribs above the ventricle in the fundamental image, which are mostly removed in the harmonic image. In state 3, the clutter is no longer

present as the tissue has been removed. The CR is increased by 14–18 dB in fundamental and harmonic images compared with state 2. However, some reverberations from the ribs inside the ventricle may be noticed in the fundamental image, which are mostly removed by HI. Further reducing the distance between the ribs and repositioning the tissue in state 4 increases the clutter level over the ultrasound images. Following this, the ventricle is almost invisible in the fundamental image and is hardly visible in the harmonic image. Furthermore, the CR has dropped to 1.3 and 5.65 dB in fundamental and harmonic cases, respectively. However, when the tissue is removed in state 5, it is again possible to visualize the ventricle, and there is an increase of 5–14 dB in CR compared with state 4. The contrast in these images is, however, lower compared with ultrasound images in states 1 and 3, where there is more distance between the ribs. The theory presented by Figure 1e was experimentally demonstrated in a water tank. In state 1 (Fig. 9), there is little energy being



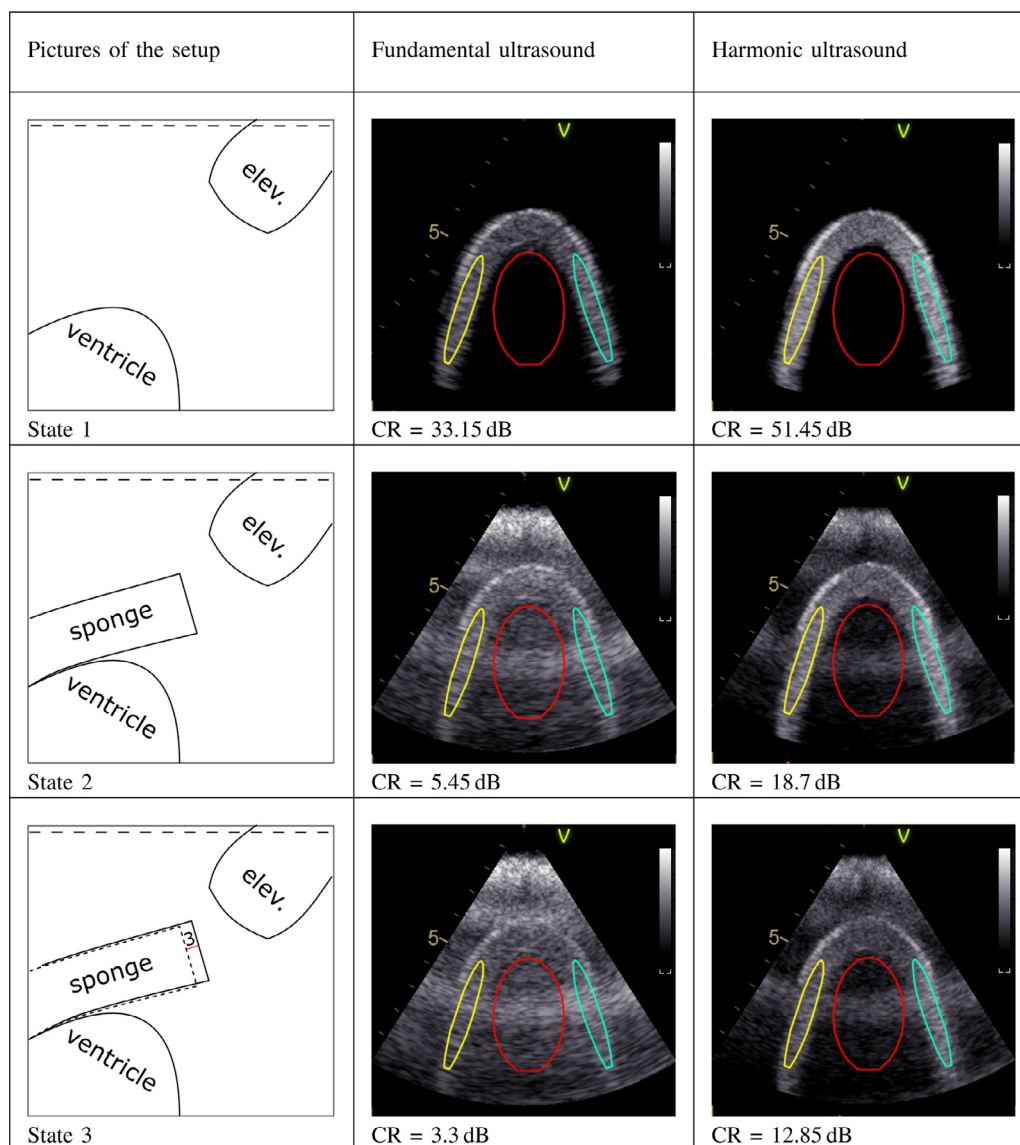


Fig. 6. Case III: Reproducing clutter noise in a water tank using a piece of sponge in elevation to simulate the effect of the lung. A synthetic ventricle is imaged by an M5Sc-D transducer in three different states. A drawing of the setup in each state is shown in the first column. The sponge in state 3 is moved 3 mm to the right compared with state 2. The water level is drawn by the dashed lines. Fundamental and harmonic ultrasound images taken in each state are shown in the second and third columns. Contrast ratios between the ventricle walls and the chamber are given under each ultrasound image. CR = contrast ratio; elev. = elevation.

deflected at the ribs. Therefore, the ventricle can clearly be seen in the fundamental and harmonic ultrasound images. In state 2, where there is a shorter distance between the ribs, the beam is partially blocked and deflected toward the sponge (representing the lung), which is placed close to the ventricle. In the fundamental ultrasound image, the ventricle is covered by clutter arising from the sponge. HI removes some of the clutter and makes it possible to see the ventricle again; however, the CR in this image is 23 dB lower compared with state 1. In state 3, following removal of the sponge, the clutter is no longer present.

Thus, the CR is increased by 14–17 dB in fundamental and harmonic images compared with state 2. The images and CR values in state 4 show that placing a layer of fat and muscle above the ribs in this case does not increase the clutter.

Figure 10 shows the recorded elevational beamprofiles with the ribs in 4 different states. A picture of the transducer and the ribs in the corner of each beamprofile shows how the ribs were positioned in each case and the horizontal distance between them in millimeters. In Figure 10a, where there is almost no interaction between

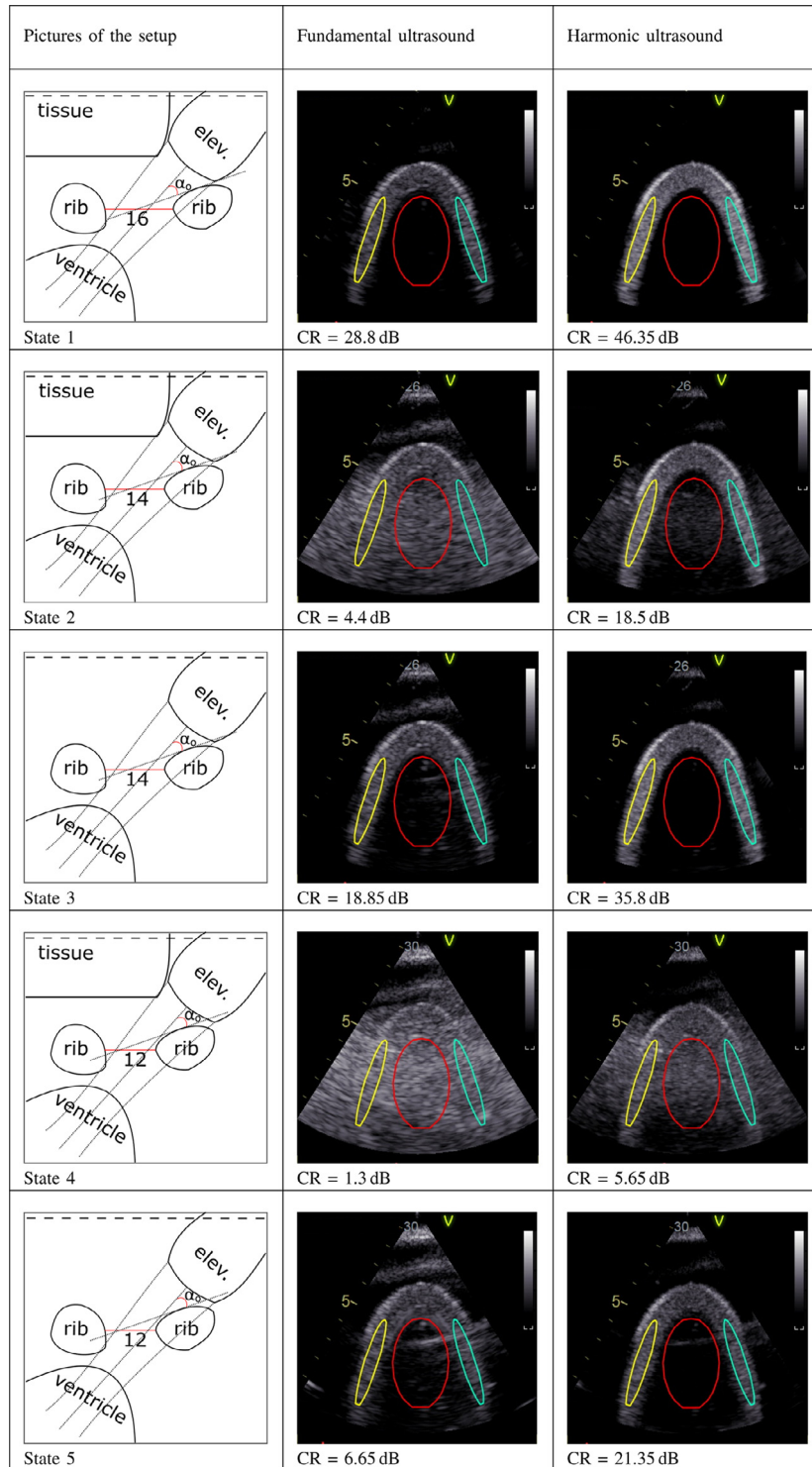


Fig. 7. Case IV: Reproducing clutter noise in a water tank using two pieces of pig ribs and a complex layer of skin, fat and muscle. A synthetic ventricle is imaged by an M5Sc-D transducer in five different states. A drawing of the setup in each state is shown in the first column. The distance between the ribs is given in millimeters, and the water level is drawn by the dashed lines. There is an angle of 35 degrees between the ultrasound beam and the right rib surface where it is hit. This is shown as  $\alpha_0$ . The approximate beam limits are drawn by dotted lines for comparison between the states. Fundamental and harmonic ultrasound images taken in each state are shown in the second and third columns. Contrast ratios between the ventricle walls and the chamber are given under each ultrasound image. CR=contrast ratio; elev. =elevation.

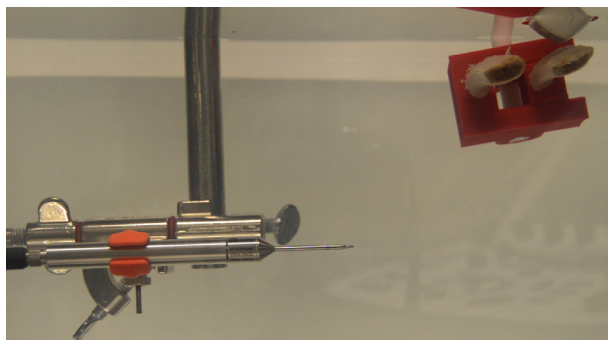


Fig. 8. An image of the setup used to measure the elevational beamprofile of an M5Sc-D transducer in a water tank while two ribs are placed in front of it. The transducer in the elevation direction with the ribs can be seen in the upper right corner of the image. The image also shows the hydrophone mounted on a robot arm.

the ribs and the beam, the expected elevational beamprofile of the transducer can be observed. Comparing the initial beamprofile with the one in Figure 10b, where the distance between the ribs is slightly reduced, verifies that ribs can behave as specular reflectors when they block the beam. The transmit beam in this case is split in two, and part of the energy is taking a new path outside the chest. The beam profile in Figure 10c shows that further reduction of the distance between the ribs results in an increasing amount of the energy being deflected out of its intended path. In the last measurement, the ribs are slightly rotated, making the angle between the beam and the rib surface smaller (see Fig. 1d, 1e and the angles  $\alpha_o$  and  $\alpha_i$ ). By comparing the last beamprofile in Figure 10d with the ones in Figure 10 (b, c), we observe how a smaller beam-to-rib angle affects the direction of the path of the ultrasound beam. Note that the deflected energy is now directed inside the rib cage.

*In vivo* examples are shown in Videos 3 to 8. Videos 3 and 4 show two echocardiograms of volunteer A. Videos 5 and 6 show echocardiograms of volunteers B and C, respectively. The last two videos (7 and 8) show two echocardiograms of volunteer D.

## DISCUSSION

### Case I

The results in Figure 4 show how a thick layer of skin, fat and muscle adds clutter over the heart image. This clutter is generated because of both aberration and reverberation from the tissue. Because of the distortion of the wavefront in the tissue, the spatial resolution of the ventricle image is reduced in state 2 compared with state 1. The effect of reverberations can also be seen in the near field of state 2 and over the whole image in state 3. The echocardiogram of volunteer C in Video 6 shows

an example of near-field clutter generated at layers of skin, fat and muscle. This clutter is relatively static with only a limited movement due to displacement of the apical region of the heart.

### Case II

In Figure 5, one can notice that HI in state 2 is not able to remove the clutter formed over the right side of the ventricle. This is due to the high difference in acoustic impedance of water (soft tissue) and air inside the sponge (lung), resulting in almost complete reflection of energy at their interface. This reflection occurs multiple times, causing high-energy reverberations that are also present in the second harmonic band and therefore in the harmonic ultrasound image. This type of clutter is seen in the echocardiograms of volunteer A in Videos 3 and 4. When the volunteer inhales and holds his breath (Video 3), the right side of the echocardiogram remains cluttered. However, in the second echocardiogram of volunteer A (Video 4), the clutter moves out of the sector while the volunteer exhales. Note that the clutter in this example flickers while moving out of the sector.

### Case III

The results of experiment 3 in Figure 6 show how blocking of the transducer in the elevation direction by lung tissue results in a cluttered ultrasound image. In this case, HI removes some of the clutter and increases the image contrast. This is due to the fact that the unblocked part of the beam contains reflections from the ventricle that dominate the reverberations in the harmonic band. The stronger bands of clutter are due to reverberations between the transducer and the sponge. However, the relatively weaker clutter between the bands is due to the reverberations inside and between air-filled cavities of the sponge. The clutter seen in this case is comparable to the one of volunteer D in Video 7. The clutter in this echocardiogram covers the whole sector and flickers (similar to the one from volunteer A).

### Beamprofiles

The results from beamprofile measurements in Figure 10 show how the rib positioning and orientation affect the path of the ultrasound energy. The beam width at the ribs' location is about 12 mm. However, since there is an angle of 50 degrees between the beam and the ribs, the effective beam width is about 16 mm. In Figure 10b, it can be seen that the deflected part of the beam has about 5 dB less energy than the main lobe. In Figure 10c, where there is a shorter distance between the ribs, the deflected energy has almost the same level as the main lobe. Therefore, this deflected part of the energy can make a strong clutter over the image if it reaches tissues outside the rib cage, such as skin and

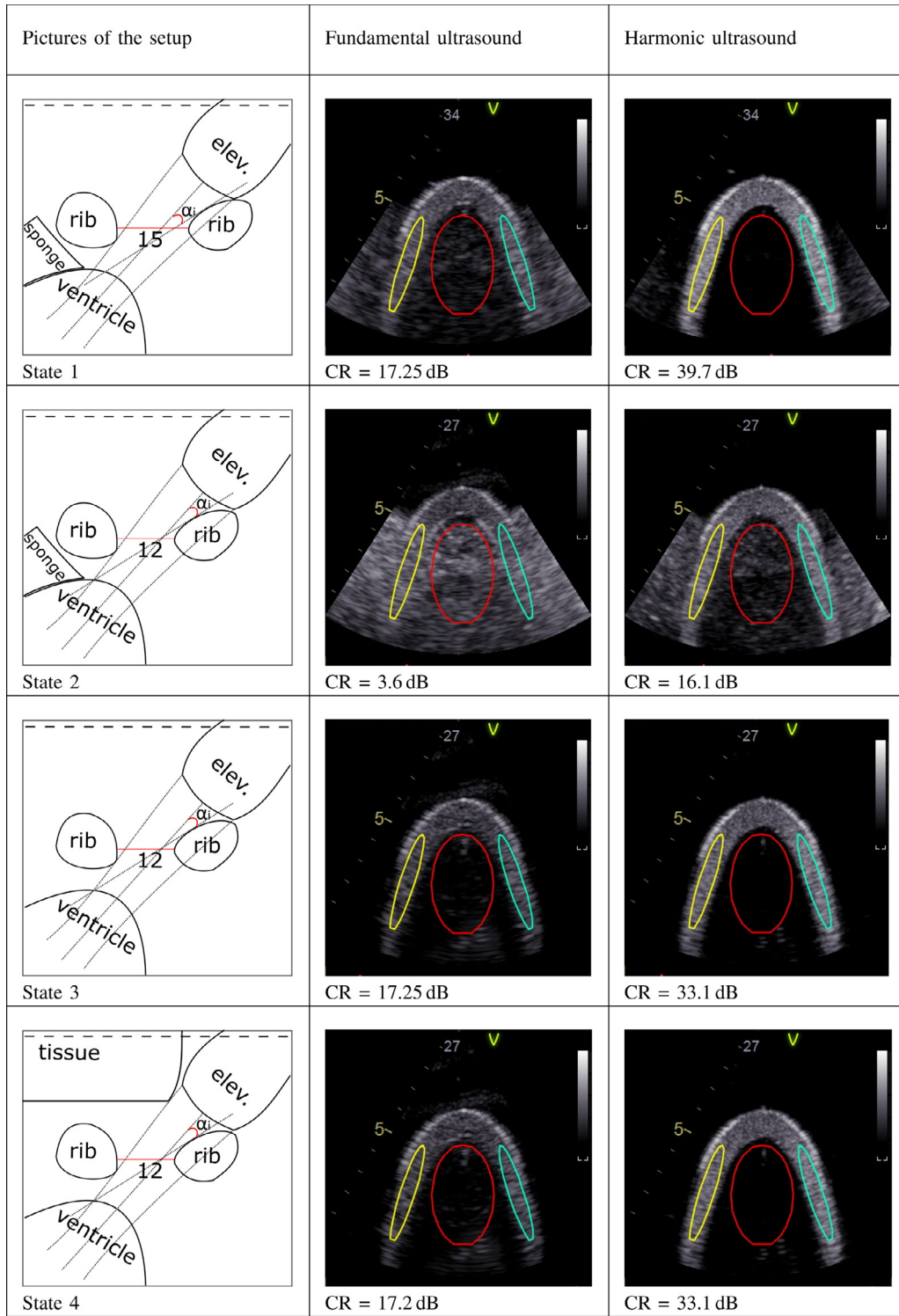


Fig. 9. Case V: Reproducing clutter noise in a water tank using two pieces of pig ribs and a piece of sponge to simulate the effect of the lung. A synthetic ventricle is imaged by an M5Sc-D transducer in four different states. A drawing of the setup in each state is shown in the first column. The distance between the ribs is given in millimeters, and the water level is drawn by the dashed lines. There is an angle of 15 degrees between the ultrasound beam and the right rib surface where it is hit. This is shown as  $\alpha_i$ . The approximate beam limits are drawn by dotted lines for comparison between the states. Fundamental and harmonic ultrasound images taken in each state are shown in the second and third columns. Contrast ratios between the ventricle walls and the chamber are given under each ultrasound image. CR = contrast ratio; elev. = elevation.

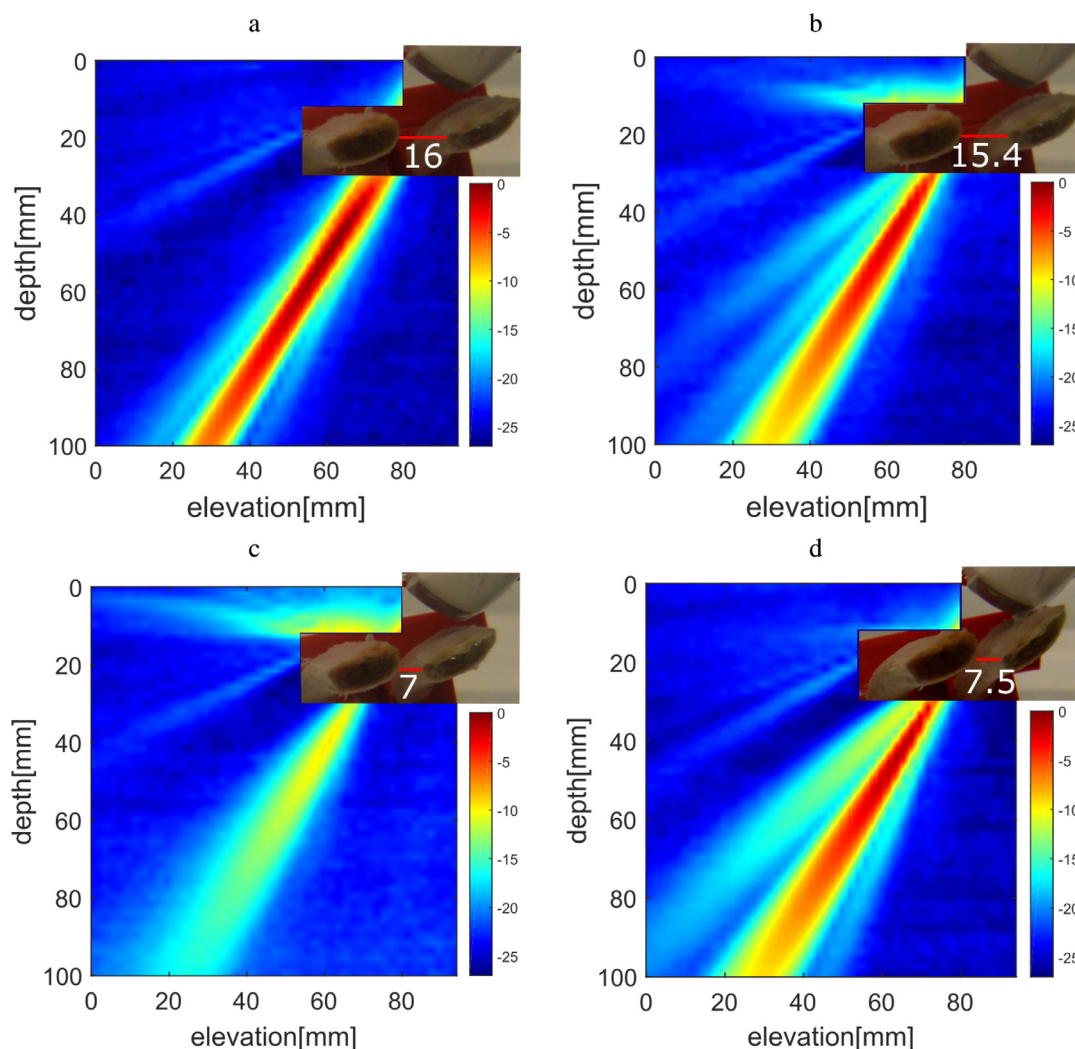


Fig. 10. The elevational beamprofile of an M5Sc-D transducer connected to a Vivid E95 ultrasound scanner in the presence of two pieces of pig ribs in front of the transducer in four different states. The image of the transducer and the ribs with their distance in millimeters at the corner of each image shows how they were placed while measuring the beamprofiles. In (a) the ribs are not blocking the transducer. In (b) the distance between the ribs is reduced so that the transducer gets partially blocked in the elevation direction by the right rib. The distance between the ribs is further reduced in (c) to block more of the aperture in the elevation direction. The orientation of the right rib is changed in (d) while it is still partially blocking the transducer.

subcutaneous fat. In Figure 10a, the deflected part of the beam has an energy level of about 10 dB lower than the main lobe. This can be enough to produce clutter after reaching an echogenic tissue like the lung. These measurements confirm the basis of our hypotheses presented in the theory section by Figure 1 (d, e).

#### Case IV

In experiment 4, the ribs and the transducer were placed in a similar way as in Figure 10 (a–c). The ventricle was placed where the main lobe of the beam was measured in Figure 10a, and a layer of skin, fat and muscle was placed where the blocked part of the energy was deflected to in

Figure 10 (b, c). The results of this experiment confirm the possibility of increased clutter in echocardiography because of reverberations from subcutaneous fat *via* specular reflection at the ribs. The clutter seen in Figure 7 is comparable to the echocardiogram of volunteer B in Video 5. In this *in vivo* example, the clutter band around a 5-cm depth moves according to a gentle push on the chest wall at about a 5-cm distance from the transducer.

#### Case V

In experiment 5, the ventricle was placed where the main lobe of the beam was measured in Figure 10a, and the sponge was placed where the blocked part of the energy

was deflected to in Figure 10d. The results of this experiment confirm the possibility of increased clutter in echocardiography due to reverberations from the lung *via* specular reflection at the ribs. The clutter seen in Figure 9 can be compared to the clutter in the echocardiogram of volunteer D in Video 7. Note that when the skin and fat layer is placed above the ribs in state 4, the ultrasound images are almost unchanged compared with state 3. This is as expected since the ultrasound beam is not being deflected out of the rib cage in this case. Hence, there is no signal coming from the tissue above the ribs. As explained in the theory section, the source of clutter after deflection of energy inside the chest can also be out-of-scan-plane heart tissue. An example of this type of clutter can be seen in the second echocardiogram of volunteer D in Video 8, where the clutter inside the left ventricle moves with the movement of the heart.

The harmonic ultrasound images and videos are obtained by bandpass filtering the received signals. Since we don't have the detailed information about how these filters are designed in the clinical scanner that we used, we cannot strictly exclude that part of the fundamental energy may leak through the harmonic image. However, even assuming that the harmonic images are not generated from pure harmonic energy, the mentioned mechanisms for generation of clutter that is seen in ultrasound images are still valid.

Although the focus of this study has been on apical four-chamber view echocardiograms, the same concepts can be extended to other views and explain the clutter origin in some other situations. The difference would then be which part of the beam is blocked and which part of the image is cluttered because of that blockage. We mostly concentrate on the clutter that is generated because of reverberations. However, in most of the examined cases, reverberation is not the only cause of the clutter, meaning that other clutter-generation mechanisms, such as aberration and side lobes, are also present in these cases.

Some studies have been carried out on the detection and compensation of blocked elements by highly reflective tissues, such as ribs and lungs. An algorithm using multiple receive beams for minimizing the effect of blocked elements on point spread function was developed by Li et al. (1993) and Li and O'Donnell (1994). In a recent study (Jakovljevic et al. 2017b), a method for detection of the elements blocked by the ribs, based on the amplitude and the cross correlation of the received signals, was developed. This method was applied to synthetic aperture data from an *ex vivo* experiment on a section of canine chest (Jakovljevic et al. 2017a). An average drop of 5 dB in reverberation clutter level was achieved by turning off the blocked elements. These methods can potentially improve the quality of the cardiac ultrasound images that are cluttered because of rib blockage. The clutter that is generated at out-of-scan-plane tissues could be suppressed by manipulating the beamprofile in the

elevation direction. This can be accomplished using 2-D matrix array technology.

## CONCLUSIONS

We present five scenarios for clutter generation in apical four-chamber view cardiac ultrasound images based on reverberations from structures within the examined body. These include moving structures, such as the heart and lungs, or stationary structures, such as skin, fat and bone. We discovered that these reverberations can also be generated at structures lying outside the imaging plane if the ultrasound beam gets deflected by the ribs. All the presented scenarios are demonstrated by water tank experiments, where we reproduce clutter in *in vitro* setups. The results of the experiments are supported by *in vivo* recordings.

We also show that the appearance of clutter varies according to the structure of origin. We see a more static clutter from stationary structures, while the clutter originated at the left lung moves with the respiration and the clutter from out-of-scan-plane heart tissue moves with the heart cycle.

Reducing the clutter from cardiac ultrasound images of difficult-to-image patients can reduce the need for contrast echocardiography and referrals to more expensive imaging methods. In order to suggest a method that efficiently reduces clutter, it is important to understand possible mechanisms that generate the clutter. The results of this study suggest that one would benefit from potential algorithms or transducer designs that can detect and correct for the beam-rib interaction. These results can also help cardiologists to better understand the source of clutter while acquiring ultrasound images. Cardiologists can apply this knowledge to change the position of the transducer in order to acquire better images.

*Acknowledgments*—This research was supported by the Center for Innovative Ultrasound Solutions (CIUS) and the Research Council of Norway, Project Code 237887. The authors would like to thank Svein-Erik Måsøy and Bastien Denarie for proofreading the article and Nancy Eik-Nes for providing language help. We would also like to thank Nor-tura Norway for providing us with animal parts.

## SUPPLEMENTARY MATERIALS

Supplementary material associated with this article can be found in the online version at <https://doi.org/10.1016/j.ultrasmedbio.2019.01.010>.

## REFERENCES

- Bell MAL, Goswami R, Trahey GE. Clutter reduction in echocardiography with short-lag spatial coherence (SLSC) imaging. In: Proceedings of the Ninth IEEE International Symposium on Biomedical Imaging. Barcelona, Spain: IEEE; 2012. p. 1116–1119. <https://ieeexplore.ieee.org/document/6235755>.
- Chirillo F, Pedrocco A, Leo AD, Bruni A, Totis O, Meneghetti P, Stritoni P. Impact of harmonic imaging on transthoracic echocardiographic identification of infective endocarditis and its complications. *Heart J* 2004;91:329–333.

- Dahl JJ, Sheth NM. Reverberation clutter from subcutaneous tissue layers: Simulation and *in vivo* demonstrations. *Ultrasound Med Biol* 2014;40:714–726.
- Fink M. Time reversal of ultrasonic fields. I. Basic principles. *IEEE Trans Ultrason Ferroelectr Freq Control* 1992;39:555–566.
- Flynn BC, Spellman J, Bodian C, Moitra VK. Inadequate visualization and reporting of ventricular function from transthoracic echocardiography after cardiac surgery. *J Cardiothorac Vasc Anesth* 2010;24:280–284.
- Goldberg BB, Liu JB, Forsberg F. Ultrasound contrast agents: A review. *Ultrasound Med Biol* 1994;20:319–333.
- Gottdiener JS, Bednarz J, Devereux R, Gardin J, Klein A, Manning WJ, Morehead A, Kitzman D, Oh J, Quinones M, Schiller NB, Stein JH, Weissman NJ. American Society of Echocardiography recommendations for use of echocardiography in clinical trials. *J Am Soc Echocardiogr* 2004;17:1086–1119.
- Hinkelman LM, Szabo TL, Waag RC. Measurements of ultrasonic pulse distortion produced by human chest wall. *J Acoust Soc Am* 1997;101:2365–2373.
- Hinkelman LM, Mast TD, Metlay LA, Waag RC. The effect of abdominal wall morphology on ultrasonic pulse distortion. Part I. Measurements. *J Acoust Soc Am* 1998;104:3635–3649.
- Jakovljevic M, Bottenus N, Kuo L, Kumar S, Dahl JJ, Trahey GE. Blocked elements in 1-D and 2-D arrays—Part II: Compensation methods as applied to large coherent apertures. *IEEE Trans Ultrason Ferroelectr Freq Control* 2017;64:922–935.
- Jakovljevic M, Pinton GF, Dahl JJ, Trahey GE. Blocked elements in 1-D and 2-D arrays—Part I: Detection and basic compensation on simulated and *in vivo* targets. *IEEE Trans Ultrason Ferroelectr Freq Control* 2017;64:910–921.
- Kurt M, Shaikh KA, Peterson L, Kurrelmeyer KM, Shah G, Nagueh SF, Fromm R, Quinones MA, Zoghbi WA. Impact of contrast echocardiography on evaluation of ventricular function and clinical management in a large prospective cohort. *JACC* 2009;53:802–810.
- Ledesma-Carbayo MJ, Mahia-Casado P, Santos A, Perez-David E, Garcia-Fernandez MA, Desco M. Cardiac motion analysis from ultrasound sequences using nonrigid registration: Validation against doppler tissue velocity. *Ultrasound Med Biol* 2006;32:483–490.
- Lediju MA, Trahey GE, Byram BC, Dahl JJ. Short-lag spatial coherence of backscattered echoes: Imaging characteristics. *IEEE Trans Ultrason Ferroelectr Freq Control* 2011;58:1377–1388.
- Li PC, Flax SW, Ebbini ES, O'Donnell M. Blocked element compensation in phased array imaging. *IEEE Trans Ultrason Ferroelectr Freq Control* 1993;40:283–292.
- Li PC, O'Donnell M. Efficient two-dimensional blocked element compensation. *Ultrasound Imaging* 1994;16:164–175.
- Lin F, Waag RC. Estimation and compensation of ultrasonic wavefront distortion using a blind system identification method. *IEEE Trans Ultrason Ferroelectr Freq Control* 2002;49:739–755.
- Liu DL, Waag RC. Correction of ultrasonic wavefront distortion using back-propagation and a reference waveform method for time-shift compensation. *J Acoust Soc Am* 1994;96:649–660.
- Main ML. Ultrasound contrast agent safety: From anecdote to evidence. *JACC: Cardiovasc Imaging* 2009;2:1057–1059.
- Mast TD, Hinkelman LM, Orr MJ, Waag RC. The effect of abdominal wall morphology on ultrasonic pulse distortion. Part II. Simulations. *J Acoust Soc Am* 1998;104:3651–3664.
- Mast TD, Hinkelman LM, Metlay LA, Orr MJ, Waag RC. Simulation of ultrasonic pulse propagation, distortion, and attenuation in the human chest wall. *J Acoust Soc Am* 1999;106:3665–3675.
- Matte GM, Neer PLMJV, Danilouchkine MG, Huijssen J, Verweij MD, Jong ND. Optimization of a phased-array transducer for multiple harmonic imaging in medical applications: Frequency and topology. *IEEE Trans Ultrason Ferroelectr Freq Control* 2011;58:533–546.
- Noble JA, Boukerroui D. Ultrasound image segmentation: A survey. *IEEE Trans Med Imaging* 2006;25:987–1010.
- Perperidis A. Postprocessing approaches for the improvement of cardiac ultrasound B-mode images: A review. *IEEE Trans Ultrason Ferroelectr Freq Control* 2016;63:470–485.
- Pinton GF, Trahey GE, Dahl JJ. Erratum: Sources of image degradation in fundamental and harmonic ultrasound imaging: A nonlinear, full-wave, simulation study. *IEEE Trans Ultrason Ferroelectr Freq Control* 2011;58:1272–1283.
- Porter TR, Xie F. Transient myocardial contrast after initial exposure to diagnostic ultrasound pressures with minute doses of intravenously injected microbubbles. *Circulation* 1995;92:2391–2395.
- Seo CH, Yen JT. Sidelobe suppression in ultrasound imaging using dual apodization with cross-correlation. *IEEE Trans Ultrason Ferroelectr Freq Control* 2008;55:2198–2210.
- Spencer KT, Bednarz J, Rafter PG, Korcarz C, Lang RM. Use of harmonic imaging without echocardiographic contrast to improve two-dimensional image quality. *Am J Cardiol* 1998;82:794–799.
- Wei K, Mulvagh SL, Carson L, Davidoff R, Gabriel R, Grimm RA, Wilson S, Fane L, Herzog CA, Zoghbi WA, Taylor R, Farrar M, Chaudhry FA, Porter TR, Irani W, Lang RM. The safety of deFinity and Optison for ultrasound image enhancement: A retrospective analysis of 78,383 administered contrast doses. *J Am Soc Echocardiogr* 2008;21:1202–1206.
- World Health Organization. The top 10 causes of death. Available at: <http://www.who.int/mediacentre/factsheets/fs310/en/>. Accessed July 1, 2018.